In situ production of nickel/graphitic carbon nanofiber composites and application in catalytic hydrodechlorination

Mark A. Keane[a,*] and Patricia M. Patterson[b]

[a]*Department of Chemical and Materials Engineering, University of Kentucky, Lexington, KY 40506, USA*
[b]*Center for Applied Energy Research, University of Kentucky, Lexington, KY 40506, USA*

Received 20 July 2004; accepted 18 September 2004

The action of Ni/SiO_2 in the gas phase hydrodechlorination (at 573 K) of chlorobenzene, 1,3-dichlorobenzene and 1,3,5-trichlorobenzene is compared with that of a $Ni/SiO_2 + C$ composite. The latter was prepared *in situ* by the decomposition of chlorobenzene at 873 K to generate graphitic carbon nanofibers bearing Ni particles at the fiber tips. The Ni/SiO_2 and $Ni/SiO_2 + C$ (with varying C content) catalysts have been characterized by TEM, SEM, XRD, and H_2 chemisorption. While the $Ni/SiO_2 + C$ system delivered a lower initial fractional dechlorination, the composite outperformed the starting Ni/SiO_2 in terms of long-term activity, an effect that is linked to the structural characteristics.

KEY WORDS: carbon nanofibers; Ni/SiO_2; chlorobenzene decomposition; $Ni/SiO_2 + C$ composite; hydrodechlorination.

Introduction

It is accepted that catalytic hydrodechlorination (HDC), in common with most hydrogenolysis reactions, is strongly influenced by the electronic structure of the active metal sites [1]. Previous work conducted in this laboratory [2–4] has demonstrated that nano-scale supported Ni is highly effective in the HDC of concentrated chlorinated gas streams. The potential application of catalytic HDC as an environmental remediation methodology has provided the impetus for this work, which is aimed at the development of highly active and selective supported metal catalysts to transform toxic halogenated waste into (environmentally benign) reusable compounds. Chlorobenzene (CB) has been the most widely adopted model haloarene reactant to assess gas phase HDC activity over Pd [5], Pt [6], Rh [5] and Ni [7] catalysts. The mechanism of C–Cl bond hydrogenolysis is still unresolved and while an unambiguous link between catalyst structure and HDC performance has yet to be established, recent studies [8–10] point to higher specific HDC activities associated with larger supported Pd and Ni particles. Catalyst deactivation is a common feature in the HDC of both aliphatic and aromatic reactants over an array of supported metal catalysts, an effect that has been attributed to carbon deposition [6] and/or surface poisoning by HCl [11] and/or metal sintering [12]. There is some evidence in the literature [13] that larger metal particles are more resistant to HCl poisoning.

* To whom correspondence should be addressed.
E-mail: makeane@engr.uky.edu

The nature of the support can influence HDC activity/selectivity and/or stability. In the latter case, the support must not suffer any structural collapse due to the corrosive effects of high HCl concentrations at elevated temperatures. Activated carbon (AC), as support material for Pd, is resistant to deleterious HCl effects [14]. We have recently recorded [10] higher specific CB HDC rates over Ni/AC when compared with Ni/SiO_2, Ni/Al_2O_3 and Ni/MgO, an effect that we attributed to combined Ni size/support interaction effects. While the use of carbon nanofibers as metal supports is attracting the interest of the catalysis community [15], their application in HDC has yet to be reported in the literature. Carbon nanofibers offer a high aspect ratio graphitic surface on which to disperse the active metal phase [16]. Such carbonaceous materials can be readily synthesized *via* catalytic hydrocarbon decomposition and tailor-made to desired specifications, in terms of lattice orientation and mechanical/chemical/electrical properties [17]. The active metal phase is subsequently introduced by standard preparative routes such as wetness impregnation, ion exchange or deposition/precipitation [16]. Highly specific metal/nanofiber interactions have been proposed to induce distinct activity/selectivity behavior when compared with corresponding amorphous carbon and oxide supported metals, notably in hydrogenation reactions [15,18]. In this paper we consider a novel *in situ* synthesis of a Ni/carbon nanofiber composite and report, for the first time, the application of this material to promote chloroarene HDC. We have demonstrated elsewhere [19] that the passage of CB in a stream of hydrogen over

1011-372X/05/0100–0033/0

Ni/SiO_2 at 873 K results in appreciable growth of carbon fibers bearing Ni particles at the fiber tips. The catalytic performance of this Ni/carbon nanofiber composite in the HDC of CB, 1,3-dichlorobenzene (1,3-DCB) and 1,3,5-trichlorobenzene (1,3,5-TCB) is compared herein with the action of the starting Ni/SiO_2, the dependence of HDC activity/stability on the duration of carbon growth is examined and linked to structural characteristics.

Experimental procedure

Catalyst preparation, activation and HDC reaction

The Ni/SiO_2 catalyst was prepared by impregnation of a fumed silica support (Aldrich) with a 2-butanolic solution of $Ni(NO_3)_2$ to yield a 7.2% w/w Ni loading, determined by inductively coupled plasma-optical emission spectrometery (ICP-OES, Vista-PRO, Varian Inc.). The catalyst precursor was sieved (ATM fine test sieves) into a batch of 100 μm average particle diameter, loaded into a fixed bed tubular quartz reactor (i.d. = 1.25 cm) and activated by heating at 10 K min^{-1} in 60 cm^3 min^{-1} (Brooks mass flow controller) dry H_2 (99.999%) to 873 K, which was maintained for 12 h. Carbon growth *via* CB decomposition has been described in some detail elsewhere [19] but details pertinent to this study are given below. A Model 100 (kd Scientific) microprocessor controlled infusion pump was used to deliver the C_6H_5Cl feed, *via* a glass/teflon air-tight syringe and teflon line at a fixed calibrated flow rate in a co-current flow of H_2; inlet H_2/C_6H_5Cl = 12.5 mol/mol with a gas hourly space velocity (GHSV) = 4×10^3. A layer of quartz wool above the catalyst bed ensured that the reactants were vaporized and reached reaction temperature before contacting the catalyst. The reaction temperature (873 ± 1 K) was monitored continuously by means of a thermocouple inserted in the catalyst bed. The reactor effluent was frozen in a liquid nitrogen trap for subsequent capillary GC analysis (Perkin–Elimer Auto System XL/FID/DB-1 50 m × 0.20 mm i.d., 0.33 μm column): overall analytical repeatability was better than ±4%. Carbon balance was monitored based on the known carbon inlet, gravimetric yield of solid carbon and chromatographic analysis of the reactor effluent using 2-octanol as internal standard.

The catalytic HDC of CB at 573 K was monitored over the freshly activated (as above) Ni/SiO_2 catalyst and the Ni/SiO_2 + C samples after CB decomposition (Δt = 1–60 min, prepared *in situ* prior to each individual HDC run). In every case the catalyst (with/without C) was cooled to 573 K in a 60 cm^3 min^{-1} H_2 stream and the HDC was monitored over a 25 h period, employing the capillary GC analysis as above. The HDC of 1,3-dichlorobenzene (1,3-DCB) and 1,3,5-trichlorobenzene (1,3,5-TCB) was also examined where the inlet hourly Cl/Ni mole ratio was maintained at 75 for each reactant. In a series of blank tests, passage of CB in a stream of H_2 through the empty reactor, i.e. in the absence of catalyst, did not result in any detectable conversion. The reactor was operated under conditions of negligible heat and mass transport constraints as discussed previously [19]. A chlorine (in the form of HCl product) mass balance was performed by passing the effluent gas through an aqueous NaOH trap ($3.5–8.0 \times 10^{-3}$ mol dm^{-3}, kept under constant agitation at ≥300 rpm) with independent pH (Hanna HI Programmable Printing pH Bench-Meter) and potentiometric (Metrohm Model 728 Autotitrys) analyses. Each catalytic run was repeated up to six times and the reaction data quoted in this paper represent average values:the carbon content and HDC activities were reproducible to within ±8%. The degree of dechlorination (x_{Cl}) is given by

$$x_{Cl} = \frac{[HCl]_{out}}{[Cl_{org}]_{in}} \quad (1)$$

where $[Cl_{org}]$ represents the concentration (mol dm^{-3}) of chlorine associated with the aromatic feed; in and out refer to the inlet and outlet reactor streams, respectively. Selectivity is defined as

$$S_{benzene}(\%) = \frac{[benzene]_{out}}{[1,3,5-TCB]_{in} - [1,3,5-TCB]_{out}} \times 100 \quad (2)$$

taking, as an example, benzene production from 1,3,5-TCB. After activation/catalysis, the catalyst was flushed for 1 h in He, cooled to room temperature and passivated in (40 cm^3 min^{-1}) 2% v/v O_2/He for subsequent off-line characterization.

Catalyst characterization

The BET surface area and H_2 chemisorption associated with the activated/passivated Ni/SiO_2 and Ni/SiO_2 + C samples were determined using the commercial CHEM-BET 3000 (Quantachrome) unit. The total surface area was recorded in a 30% v/v N_2/He flow; pure N_2 (99.9%) served as the internal standard. After outgas at 523 K for 30 min, at least two cycles of N_2 adsorption–desorption in the flow mode were employed using the standard single point BET method. Directly after BET measurement, the samples were activated as above, cooled to room temperature and subjected to H_2 chemisorption using a pulse (50–100 μL) titration procedure with on-line TCD analysis; BET area/H_2 uptake values were reproducible to within ±5%. High resolution transmission electron microscopy (HRTEM) was carried out using a JEOL-2010 TEM/STEM equipped with energy dispersive X-ray (EDX) detector (Oxford Instruments) operated at an accelerating voltage of 200 kV. Specimens for TEM analysis were prepared by ultrasonic dispersion in *n*-butanol where a drop of the resultant suspension was evaporated on a

holey carbon support grid. Analysis by scanning electron microscopy (SEM) was carried out using a Hitachi S900 field emission SEM, operated at an accelerating voltage of 18 kV; the sample was deposited on a standard aluminum SEM holder and coated with gold. Powder X-ray diffractograms (XRD) were recorded with a Philips X'Pert instrument using nickel filtered Cu Kα radiation. The samples were mounted in a low background sample holder and scanned at a rate of 0.02° step^{-1} over the $20 \leq 2\theta \leq 85°$ range with a scan time of 5 s step^{-1}. The diffractograms were compared with the JCPDS-ICDD [20] references for identification purposes.

Results and discussion

(a) *Synthesis and characterization of $Ni/SiO_2 + C$ composite*

The catalytic growth of ordered carbon nanofibers is now established *via* hydrocarbon decomposition over unsupported [21] and supported [22–24] Ni catalysts. The commonly accepted growth mechanism [17,21] involves hydrocarbon decomposition on the top surface of the metal particle followed by a diffusion of carbon atoms into the metal with precipitation at other facets of the particle to yield the fiber which continues to grow until the metal particle becomes poisoned or completely encapsulated by carbon. It has been proposed [17,25] that the carbon dissolves to form a sub-stoichiometric metal carbide prior to fiber formation. The dimensions of the seed metal particles determine the width of the fibrous product while the length depends largely on the duration of reaction [26]. The degree of crystalline order of the fibers is controlled by various factors including the wetting properties of the metal with graphite and the crystallographic orientation of the metal faces that are in contact with the carbon deposit, features that are ultimately reliant upon the choice of catalyst [17,21,27]. We have shown recently [19] that the yield of carbon from a CB feed (as an atypical carbon source) is significantly greater than that generated from benzene under identical conditions while the carbon fibers generated from CB are appreciably more ordered. This effect was attributed to CB/catalyst interactions leading to Ni particle restructuring that provide a chemically modified pathway to an ordered carbon product. Such a metal site restructuring may lead to distinct HDC behavior associated with the $Ni/SiO_2 + C$ composite–such is the premise on which this study is based.

Representative TEM images of the parent activated Ni/SiO_2 are shown in figure 1(a): selected area electron diffraction confirmed the presence of Ni metal with no evidence of any surface metal oxide. The supported Ni particles exhibit a rounded or spherical geometry as noted in an earlier TEM analysis of Ni/SiO_2 [28]. It has been demonstrated [29,30] that Ni/SiO_2: prepared by impregnation realizes relatively weak metal/support interactions resulting in appreciable Ni growth during activation. Indeed, the Ni particle sizes (figure 2), derived from the TEM analysis, exhibits a wide distribution (<5 to >50 nm) with a mean diameter = 17 nm (table 1). TEM analysis (figure 1(b)) of Ni/SiO_2 after 1 min on-stream contact with CB at 873 K revealed a decided facetted geometry of the Ni particles that was not apparent in the freshly activated sample. Ni particle growth was also in evidence leading to a higher mean Ni diameter i.e., 20 nm as recorded in table 1. Indeed, Ni particle growth has been reported during catalytic hydrodechlorination (under less severe reaction conditions) [3,12] and can be ascribed to a halide-induced agglomeration of Ni particles [31] due to the surface mobility of Ni–Cl species [32]. Appreciable carbon fiber growth was apparent at extended reaction times resulting in a net reduction in the % w/w Ni content but with a negligible response in BET surface area (see table 1). The representative TEM images shown in figure 1(c) illustrate the nature of the carbon growth where the occurrence of an entrapped Ni particle at the fiber tip was a feature that was common to the majority of fibers. The structural characteristics of the carbonaceous product are further demonstrated by the representative SEM images included in figure 3. Whereas the surface morphology of the parent Ni/SiO_2 that emerges from the SEM image (figure 3(a)) is featureless, the appreciable fibrous growth associated with $Ni/SiO_2 + C$ is immediately evident in figure 3(b). Where the metal interaction with the support is relatively weak, as in the case of Ni impregnated SiO_2, the pressure exerted on the metal/support interface due to fiber growth is of sufficient magnitude to extract the metal particle from the support. Indeed, repeated EDX analysis showed negligible Si presence at the fiber tip bearing the Ni or along the length of the fiber. Once the Ni particle is detached from the SiO_2 substrate, a fresh surface is exposed to the incoming feed and growth continues with the Ni particle located on the fiber tip. This can be seen from the TEM image given in figure 1(d) showing extensive fiber formation with exposed facetted metal at the fiber tips. With prolonged carbon growth, Ni sintering is particularly evident with a shift in particle size distribution to higher values (figure 2) and a consequent increase in mean Ni diameter (table 1):the Ni size distributions associated with the $Ni/SiO_2 + C$ composite samples reflects the size of the Ni particles exposed at the fiber tips. Comparable metal sintering has been reported during carbon growth from ethylene [17,18,24] decomposition over Ni/SiO_2. The considerable reduction in H_2 uptake on the composite samples, recorded in table 1, can also be linked to a corresponding increase of Ni particle size but a suppression of H_2 chemisorption may also be the result of Ni site occlusion by the fibrous growth. Moreover, Cl/catalyst interactions are known to limit the degree of H_2 chemisorption

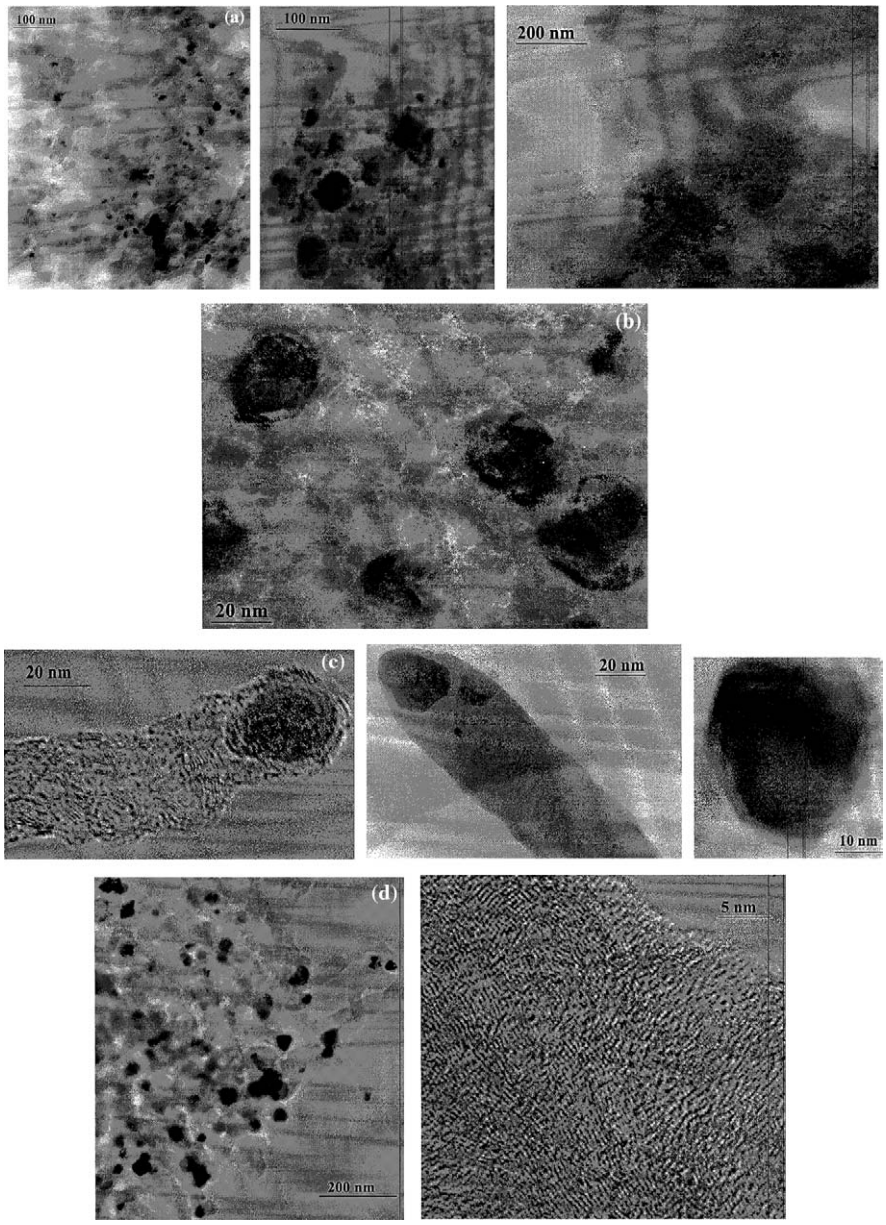

Figure 1. Representative TEM images illustrating (a) nature of the supported Ni phase in the activated unused parent Ni/SiO_2, (b) evidence of Ni particle restructuring/faceting after 1 min on-stream chlorobenzene decomposition, (c) carbon nanofiber tips bearing Ni particles after 15 min on-stream and (d) appreciable carbon growth with the presence of faceted Ni particles at the fiber tips after 60 min on-stream with high resolution TEM showing nanofiber lattice structure.

on supported Ni [33]. The X-ray diffractograms for the parent Ni/SiO_2 and composite samples (see figure 4) exhibit three peaks with characteristic d spacings = 2.0341 Å, 1.7621 Å and 1.2461 Å that correspond to the (111), (200), and (220) planes of metallic nickel, consistent with an exclusive cubic symmetry. Taking the signal at 2.0341 Å, the peak width at half height, i.e., the standard peak broadening approximation, is consistent with an increase in the average Ni particle size in the $Ni/SiO_2 + C$ composites, in agreement with the TEM/H_2 chemisorption measurements. While there was no evidence, on the basis of XRD analysis, for metal carbide formation, the XRD profiles associated with the $Ni/SiO_2 + C$ samples reveal an additional broad peak (at d = 3.4Å) for carbon growth in excess of 15 min duration. This peak coincides with that which dominates the XRD profile for a model graphite (see profile (f) in figure 4) and the d spacing agrees with the reference value [20]. The broadness of the "graphite" XRD peak associated with $Ni/SiO_2 + C$ is indicative of the presence of an amorphous carbon component [34]. The structural integrity of the carbon fibers can, however, be assessed from the HRTEM image presented in figure 1(c) where the lattice structure is in evidence with an inter-platelet spacing = ca. 0.3 nm, diagnostic of graphitic species. Taking an overview of the characterization results, the

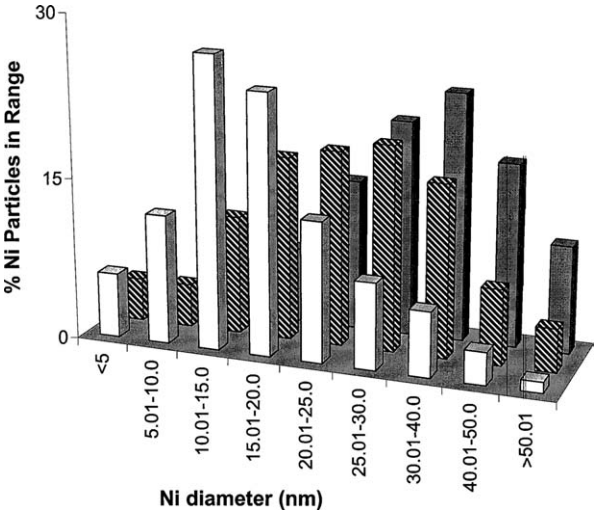

Figure 2. Nickel particle size distribution associated with the activated/passivated Ni/SiO_2: unused (open bars); after 15 min of carbon growth (hatched bars); after 60 min of carbon growth (solid bars).

metal phase in the starting Ni/SiO_2 differs from that associated with $Ni/SiO_2 + C$ in terms of Ni restructuring and sintering as a result of carbon growth with an extraction of Ni from the original SiO_2 support and incorporation into the graphitic fibers.

(b) HDC performance: Ni/SiO_2 versus $Ni/SiO_2 + C$

The fractional CB dechlorination under identical reaction conditions is illustrated in figure 5 as a function of time-on-stream for the parent Ni/SiO_2 and $Ni/SiO_2 + C$ composite samples. The HDC of CB generated benzene as the sole product with no detectable cyclohexene, cyclohexane or cyclohexyl chloride in the product stream, i.e. 100% HDC selectivity. In each case there was an initial drop in activity that was followed by a lesser decline as steady state conversion was approached. The temporal response of x_{Cl} can be expressed in terms of the empirical relationship

$$\frac{(x_{Cl} - x_0)}{(x_{25h} - x_0)} = \frac{\Delta t}{(\beta + \Delta t)} \quad (3)$$

where x_{25h} represents the fractional conversion after 25 h on-stream and β is a time scale fitting parameter.

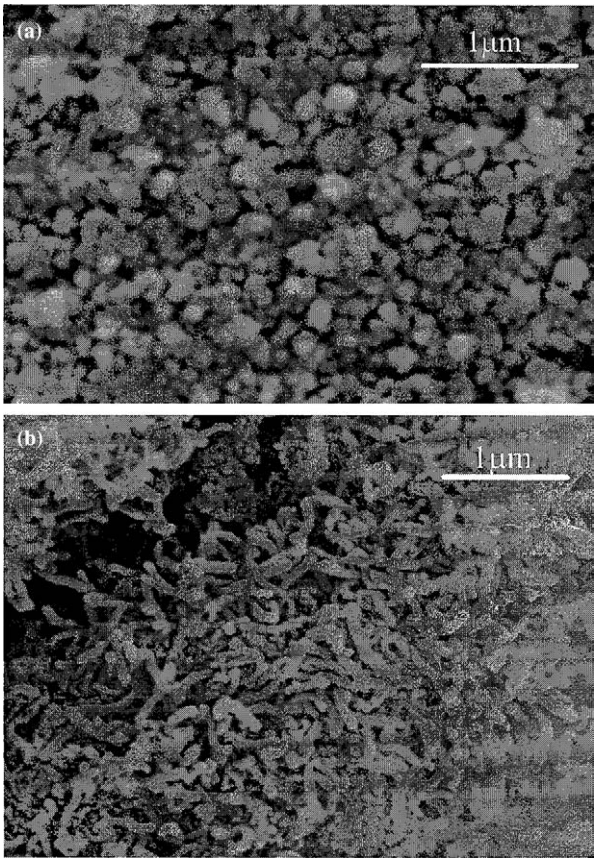

Figure 3. Representative SEM images showing structural features associated with (a) Ni/SiO_2 and (b) $Ni/SiO_2 + C$.

Fit convergence yielded values for x_0, the initial fractional dechlorination, which along with $\Delta t_{0.9}$, the time required for the conversion to decay to 90% of its initial value, are two practical indices on which to base a comparison of catalytic activity and stability:these values are recorded in table 1. The loss of HDC activity with time has been observed elsewhere and attributed to deleterious HCl/catalyst interactions [3,11,12]. While the initial fractional CB dechlorination (x_0) associated with the starting Ni/SiO_2 is certainly higher than that delivered by the $Ni/SiO_2 + C$ composites (see table 1 and figure 5), HDC activity is far more stable in the

Table 1
Ni content (% w/w) in the catalyst bed pre- and post-carbon growth, the associated BET surface areas, H_2 uptake, mean Ni particle size (d_{Ni}, from TEM analysis), the initial fractional CB dechlorination (x_0) and the time required for that value to decline by 10% ($\Delta t_{0.9}$)

Carbon growth (min)	Ni content (% w/w)	BET surface area ($m^2\ g^{-1}$)	H_2 uptake ($\mu mol\ g_{Ni}^{-1}$)	d_{Ni} (nm)	x_0	$\Delta t_{0.9}$ (min)
–[a]	7.2	195	326	17	0.40	17
1	7.2	198	43	20	0.32	26
15	4.8	206	9	27	0.28	52
30	3.5	210	10	33	0.26	95
60	2.2	200	7	37	0.25	181

[a]Freshly activated catalyst.

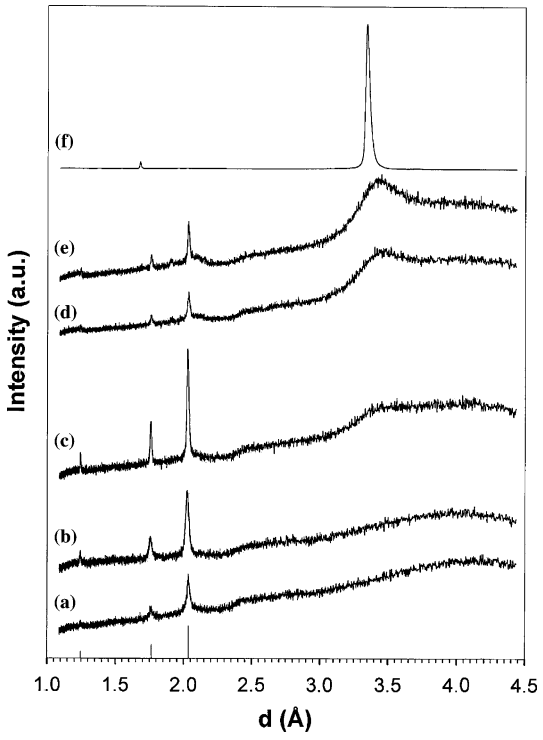

Figure 4. XRD patterns for (a) passivated Ni/SiO_2, (b) Ni/SiO_2 + C (1 min C growth), (c) $Ni/SiO_2 + C$ (15 min C growth), (d) $Ni/SiO_2 + C$ (30 min C growth), (e) $Ni/SiO_2 + C$ (60 min C growth) and (f) graphite. *Note:* the solid lines indicate peak position (with relative intensity) for cubic Ni.

latter case with associated higher $\Delta t_{0.9}$ values. Taking the family of $Ni/SiO_2 + C$ samples, initial HDC activity declines but converges to a common value (x_0) at higher C content with a concomitantly greater relative invariance with time on-stream. The latter effect is such that the $Ni/SiO_2 + C$ sample with the highest C content delivers the highest x_{25h} values. There is some, albeit limited evidence in the literature [18,35] that carbon nanofibers as structured carbon support material can modify the catalytic behavior of a supported metal phase. The nanofiber support provides exposed edge sites for anchoring the metal particles with strong electronic interactions that impact on hydrogen addition reactions [18]: such an effect has not been demonstrated for hydrogenolysis. Moreover, the studies to date have considered the support action of carbon nanofiber in conventional terms, i.e. as a substrate on which to disperse the metal phase. Our transformation of a standard Ni on SiO_2 catalyst into a nanofiber entrapped Ni material represents a distinct synthesis route to a unique supported Ni material. Nevertheless, the enhanced HDC stability associated with the $Ni/SiO_2 + C$ composites is not necessarily without precedent in that Lingaiah *et al.* [36] have prepared a Ni-carbon composite catalyst through a carbothermal reduction of a Ni exchanged resin to generate a well dispersed metal phase on an amorphous carbon support that exhibited highly stable CB HDC behavior.

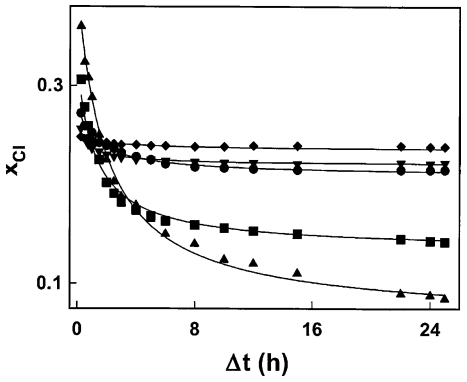

Figure 5. Fractional CB dehalogenation (x_{cl}) as a function of time-on-stream over freshly activated Ni/SiO_2 (▲) and the Ni/SiO_2 + carbon composite generated by CB decomposition after 1 min (■), 15 min (●), 30 min (▼) and 60 min (♦) on-stream. *Note:* lines represent fits to equation (3).

Table 2
Ratio of final to initial fractional dechlorination (x_{25h}/x_0) and associated benzene selectivity ($S_{benzene}$) in the HDC of 1,3-DCB and 1,3,5-TCB over Ni/SiO_2 and $Ni/SiO_2 + C$

Carbon Growth (min)	1,3-DCB			1,3,5-TCB		
	x_{25h}/x_0	$(S_{benzene})_0$	$(S_{benzene})_{25h}$	x_{25h}/x_0	$(S_{benzene})_0$	$(S_{benzene})_{25h}$
–[a]	0.18	62	16	0.11	32	8
1	0.26	54	22	0.18	27	11
15	0.59	46	32	0.43	24	14
30	0.65	43	34	0.48	23	17
60	0.68	42	36	0.51	24	16

[a]Freshly activated catalyst.

The trends established for CB HDC (lower x_0 but higher x_{25h} associated with $Ni/SiO_2 + C$) extend to the conversion of di- and tri-substituted chlorobenzenes as can be seen from the entries in table 2. The HDC of 1,3-DCB and 1,3,5-TCB over the Ni/SiO_2 and $Ni/SiO_2 + C$ catalysts generated CB and 1,3-DCB (in the case of the 1,3,5-TCB) as products of partial dechlorination as well as the fully dechlorinated benzene. A sequential removal of Cl from polychlorinated aromatics has been noted elsewhere [4,37] for reaction over supported Ni where the partially dechlorinated aromatic serves as a reactive intermediate. Fractional dechlorination (at a common inlet Cl/Ni mol ratio) decreased in the order CB > 1,3-DCB > 1,3,5-TCB, a response that can be taken as diagnostic of the deactivating influence of each Cl substituent on the ring that renders the entire halogen component less susceptible to hydrogen attack, in accordance with an electrophilic mechanism as discussed elsewhere [2,3,35]. The latter is manifested in the higher benzene selectivities generated from the DCB feed when compared with TCB (in table 2) over each catalyst. The greater HDC stability associated with the $Ni/SiO_2 + C$ system is illustrated by higher x_{25h}/x_0 values; i.e. a

greater retention of activity over prolonged reaction times. The retention of activity is such that while complete dechlorination (given by $S_{benzene}$ in table 2) is initially markedly greater for the parent Ni/SiO_2, benzene selectivity was higher for each $Ni/SiO_2 + C$ after 25 h on stream:see ($S_{benzene}$) 25 h values in table 2.

It has been shown that certain crystallographic orientation(s) of Ni favor(s) reactant decomposition while a different set of faces serves to promote the precipitation of a graphitic carbon product [17]. The decomposition of CB to generate the graphitic nanofiber can result in a restructuring of the surface Ni, creating exposed faces that present an atomic arrangement favoring dissociative/destructive chemisorption with concomitant carbon diffusion/precipitation.

Moreover, the interaction of an electronegative Cl component with surface Ni sites can induce electronic perturbations through a reduction in d-electron density of the surface Ni metal. The Ni particles extracted from the parent SiO_2 support that are incorporated in the growing fiber exhibited reduced HDC activity that is maintained over a prolonged period of reaction with the result that the *in situ* synthesized $Ni/SiO_2 + C$ ultimately outperforms the starting Ni/SiO_2.

Conclusions

The hydrogen assisted decomposition of chlorobenzene (at 873 K for a period of from 1 to 60 min) over Ni/SiO_2 was employed to generate, *in situ*, a $Ni/SiO_2 + C$ composite catalyst that exhibited greater HDC stability than that delivered by the starting Ni/SiO_2. The carbon product took the form of structured fibers typically bearing individual Ni particles at the nanofiber tips. The entrapped Ni particles exhibit a faceting and sintering when compared with the supported metal phase associated with the starting Ni/SiO_2. While the initial fractional dechlorination (of a mono-, a di- and a tri- chlorobenzene) was inhibited by carbon growth, HDC activity was largely maintained with prolonged time on-stream to ultimately exceed the level of dechlorination achieved with the parent Ni/SiO_2, which declined continually with time.

Acknowledgments

The assistance of L.D. Cherukuri and S. Palsam with the catalytic measurements is acknowledged. This work was supported in part by the National Science Foundation through Grants CTS-0218591 and CTS-0328955.

References

[1] A.Yu. Stakheev and L.M. Kustov, Appl. Catal. A: Gen. 188 (1999) 3.
[2] M.A. Keane and D.Yu. Murzin, Chem. Eng. Sci. 56 (2001) 3185.
[3] C. Park, C. Menini, J.L. Valverde and M.A. Keane, J. Catal. 211 (2002) 451.
[4] G. Pina, C. Louis and M.A. Keane, Phys. Chem. Chem. Phys. 5 (2003) 1924.
[5] B. Coq, G. Ferrat and F. Figueras, J. Catal. 101 (1986) 434.
[6] E.J. Creyghton, M.H.W. Burgers, J.C. Jansen and H. van Bekkum, Appl. Catal. A: Gen. 128 (1995) 275.
[7] G. Tavoularis and M.A. Keane, J. Mol. Catal. A: Chem. 142 (1999) 187.
[8] W. Juszczyk, A. Mallinowski and Z. Karpinski, Appl. Catal. A: Gen. 166 (1998) 311.
[9] M.A. Armendia, V. Borau, I.M. Garcia, C. Jimenez, A. Marinas, J.M. Marinas and F.J. Urbano, J. Catal. 187 (1999) 392.
[10] C. Park, C. Menini and M.A. Keane, Catal. Lett. 88 (2003) 89.
[11] J. Estellé, J. Ruz, Y. Cesteros, R. Fernandez, P. Salagre, F. Medina and J.-E. Sueiras, J. Chem. Soc., Faraday Trans. 92 (1996) 2811.
[12] A. Gampine and D.P. Eyman, J. Catal. 170 (1998) 315.
[13] Z.C. Zhang and B.C. Beard, Appl. Catal. A 174 (1998) 33.
[14] L. Prati and M. Rossi, Appl. Catal. B: Environ. 23 (1999) 135.
[15] P. Serp, M. Corrias and P. Kalck, Appl. Catal. A: Gen. 253 (2003) 337.
[16] M.L. Toebes, F.P. Prinsloo, J.H. Bitter, A.J. van Dillen and K.J. de Jong, J. Catal. 214 (2003) 78.
[17] C. Park, P.M. Patterson and M.A. Keane, Curr. Topics Colloid. Interface Sci. 5 (2002) 93.
[18] C. Park and M.A. Keane, J. Colloid. Interface Sci. 203 (2003) 183.
[19] L.D. Cherukuri, G. Yuan and M.A. Keane, Topics Catal. 29 (2004) 119.
[20] JCPDS–ICDD, PCPDFWIN, Version 2.2, (June 2001) .
[21] R.T.K. Baker, M.A. Barber, P.S. Harris, F.S. Feates and R.J. Waite, J. Catal. 26 (1972) 51.
[22] A.J.H.M. Kock, P.K. de Bokx, E. Boellaard, W. Klop and J.W. Geus, J. Catal. 96 (1985) 468.
[23] C. Park and M.A. Keane, Langmuir 17 (2001) 8386.
[24] C. Park and M.A. Keane, Chem. Phys. Chem. 2 (2001) 101.
[25] V.V. Chesnokov, V.I. Zaikovskii and R.A. Buyanov, J. Mol. Catal. A: Chem. 158 (2000) 267.
[26] T.E. Müller, D.G. Reid, W.K. Hsu, J.P. Hare, H.W. Kroto and D.R.M. Walton, Carbon 35 (1997) 951.
[27] N.M. Rodriguez, J. Mater. Res. 8 (1993) 3233.
[28] C. Park and M.A. Keane, Catal. Commun. 2 (2001) 171.
[29] P. Burattin, M. Che and C. Louis, J. Phys. Chem. B 101 (1997) 7060.
[30] M.A. Keane, Can. J. Chem. 72 (1994) 372.
[31] Y. Ohtsuka, J. Mol. Catal. 54 (1989) 225.
[32] C. Hoang-Van, Y. Kachaya and S.J. Teichner, J. Phys. Chem. B 101 (1997) 7060.
[33] D.J. Moon, M.J. Chung, K.Y. Park and S.I. Hong, Appl. Catal. A: Gen. 168 (1998) 159.
[34] S. Takenaka, H. Ogihara and K. Otsuka, J. Catal. 208 (2002) 54.
[35] T.G. Ros, D.E. Keller, A.J. van Dillen, J.W. Geus and D.C. Koningsberger, J. Catal. 211 (2002) 85.
[36] N. Lingaiah, Md. A. Uddin, A. Muto, T. Iwamoto, Y. Sakata and Y. Kusano, J. Mol. Catal. A:Chem. 161 (2000) 157.
[37] E.J. Shin and M.A. Keane, J. Chem. Technol. Biotechnol. 75 (2000) 159.